FORESTRY AND NATURAL SCIENCES

Kalle Ventola

Polarization state manipulation with sub-micron structures

Publications of the University of Eastern Finland
Dissertations in Forestry and Natural Sciences No 92

UNIVERSITY OF
EASTERN FINLAND

KALLE VENTOLA

Polarization state manipulation with sub-micron structures

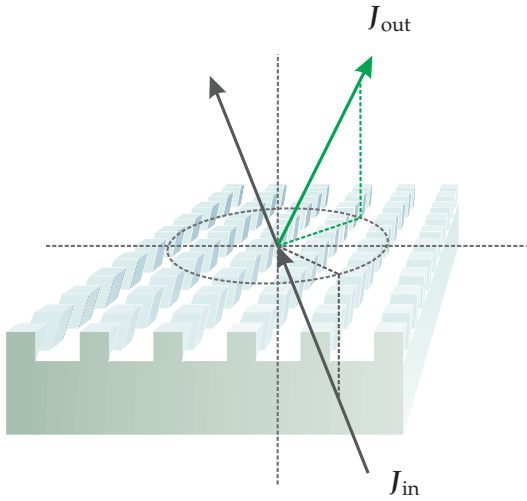

Publications of the University of Eastern Finland
Dissertations in Forestry and Natural Sciences
No 92

Academic Dissertation
To be presented by permission of the Faculty of Science and Forestry for public examination in the Auditorium M103 in the Metria Building at the University of Eastern Finland, Joensuu, on december, 5, 2012,
at 12 o'clock noon.

Department of Physics and Mathematics

Kopijyvä Oy
Joensuu, 2012
Editor: Prof. Pertti Pasanen
Prof. Kai Peiponen, Prof. Pekka Kilpelinen, Prof. Matti Vornanen

Distribution:
University of Eastern Finland Library / Sales of publications
julkaisumyynti@uef.fi
http://www.uef.fi/kirjasto

ISBN: 978-952-61-0979-4 (printed)
ISSNL: 1798-5668
ISSN: 1798-5668
ISBN: 978-952-61-0980-0 (pdf)
ISSN: 1798-5676

Author's address:
University of Eastern Finland
Department of Physics and Mathematics
P.O.Box 101
80101 Joensuu
FINLAND
email: kalle.ventola@uef.fi

Supervisors:
Professor Markku Kuittinen, Ph.D.
University of Eastern Finland
Department of Physics and Mathematics
P.O.Box 101
80101 Joensuu
FINLAND
email: markku.kuittinen@uef.fi

Associate Professor Jani Tervo, Ph.D.
University of Eastern Finland
Department of Physics and Mathematics
P.O.Box 101
80101 Joensuu
FINLAND
email: jani.tervo@uef.fi

Reviewers:
Yves Jourlin, Ph.D.
University of Saint Etienne
Lab. Hubert Curien, UMR CNRS
18, rue Prof. Benoit Lauras
42000 Saint Etienne
FRANCE
email: yves.jourlin@univ-st-etienne.fr

Janne Simonen, Ph.D.
Tampere University of Technology
Optoelectronics Research Centre
P.O.Box 692
33101 Tampere
FINLAND
email: janne.simonen@tut.fi

Opponent:
Professor Jesus Lancis Saez, Ph.D.
University Jaume I
Photonics Research Group (GROC)
12071 Castello
SPAIN
email: lancis@uji.es

ABSTRACT

This thesis is a study of microstructured optical elements which are designed to change the polarization state of incident light. A brief introduction to the electromagnetic theory of light is given, as well as the basics of grating diffraction and traditional polarization control. A method for extending the classical Jones algebra to diffractive configurations is presented as a novel way of numerical design. Fabrication of dielectric microstructures with electron beam lithography is briefly discussed, with focus on the fabrication of slanted profile gratings. Experimental results are shown about slanted structures that produce two novel linear birefringence -type effects. In addition, numerical results of a non-chiral diffraction element producing strong optical activity are presented.

Universal Decimal Classification: 535.421, 535.5, 681.7.02, 681.7.063
PACS Classification: 42.25.Fx, 42.25.Ja, 42.79.-e, 42.79.Dj, 81.07.-b, 81.16.Nd
Library of Congress Subject Headings: Optics; Polarization (Light); Refraction, Double; Optical instruments; Microstructure; Nanostructures; Diffraction gratings; Optical wave guides; Lithography, Electron beam
Yleinen suomalainen asiasanasto: optiikka; optiset laitteet; hilat; mikrorakenteet; nanorakenteet; polarisaatio; kahtaistaittuminen; elektronisuihkulitografia

Preface

I am grateful for the opportunity to work as a Ph.D. student, and I want to express my gratitude to the current and previous leaders of the department. Working here has provided me with food and shelter in this cruel world. I hope I have contributed something in return. Professor Markku Kuittinen deserves huge thanks for years of supervising and for employing me in the first place. Biggest possible thanks go to Jani Tervo. It is hard to imagine a more resourceful supervisor and a nicer boss.

I want to thank all my co-authors, especially Benfeng Bai and Samuli Siitonen. Janne Laukkanen deserves special credit for his guidance in the ”yellow lights district”.

During the last years, it has become clear I rather hang out with people than with computers and machines. Luckily, I’ve had so many great people to work with: Jarno, Jussi, Risto, Ismo, Ville, Petri, Petri, Tommi, Mikko, and all you others. Big thanks to the whole bunch!

Deep thanks for the support to mom, dad, and Elina & Karri. And last, the deepest thanks to my beloved Anni, for all the encouragement and happiness you have given me.

On a night train, November 6, 2012 *Kalle Ventola*

LIST OF PUBLICATIONS

This thesis consists of the present review of the author's work in the field of polarization optics and the following selection of the author's publications:

I N. Passilly, K. Ventola, P. Karvinen, P. Laakkonen, J. Turunen, and J. Tervo, "Polarization conversion in conical diffraction by metallic and dielectric subwavelength gratings," *Appl. Opt.* **46,** 4258–4265 (2007).

II K. Ventola, J. Tervo, P. Laakkonen, and M. Kuittinen, "High phase retardation by waveguiding in slanted photonic nanostructures," *Opt. Express* **19,** 241–246 (2011).

III K. Ventola, J. Tervo, S. Siitonen, H. Tuovinen, and M. Kuittinen, "High efficiency half-wave retardation in diffracted light by coupled waves," *Opt. Express* **20,** 4681–4689 (2012).

IV B. Bai, K. Ventola, J. Tervo, and Y. Zhang, "Determination of the eigenpolarizations in arbitrary diffraction orders of planar periodic structures under arbitrary incidence," *Phys. Rev. A*, **85**, 053808 (2012).

Throughout the overview, these papers will be referred to by Roman numerals.

In addition, studies on polarization control with microstructures have been published in articles [1, 2] in which the author has been a co-author.

AUTHOR'S CONTRIBUTION

The publications selected for this dissertation are original research papers on polarization state manipulation with microstructures.

In papers **II** and **III** the author has carried out most of the grating design and numerical analysis, all lithographical work except the reactive ion beam etching, and all optical measurements. In paper **I** the author has contributed half of the numerical analysis. In paper **IV** the author contributed significantly to the formulation and testing of the presented eigenpolarization method.

The manuscripts for papers **II** and **III** were mainly written by the author. In paper **IV** the author has written the parts about the last two examples. In paper **I** the author has contributed one third of the overall writing process.

Contents

1 Introduction

Physics, and photonics as a part of it, are basically mankinds attempts to understand the behavior of energy in nature. Technology is then mankinds way to utilize their findings, either by extrapolating from or mimicking some features of nature. A couple hundred years ago, a physicist could master the whole physics known at the time. Since then the amount and scope of scientific knowledge has exploded. Therefore, a current day Ph.D. thesis in physics deals with a ridiculously small corner of a subsegment of a segment of physics. Moreover, it is difficult to define where physics ends and technology begins. This thesis, studying the polarization of light and light interaction with microstructures, is somewhere on that border.

Photonics is the study of light. It has been shaped since the 17th century by famous physicists such as Isaac Newton, Thomas Young, James Clerk Maxwell, and also Albert Einstein [3–6]. A significant step forward in photonics was the invention and development of laser in the 1950s and 60s, an example of extrapolation from physical findings [7–9].

Polarization is a fundamental property of electromagnetic waves, such as visible light. In nature, over 100 animal species are able to perceive the polarization direction of polarized skylight, including birds who use it for navigation [10, 11]. When it comes to humans, the 17th century scientists discovered polarization by observing the birefringence of light passing through Calcite crystal, an early found example of light-matter interaction [12].

The recent development of laser- and led-sources and modern micro- and nanofabrication methods has produced whole new technologies, such as optical telecommunications and modern display devices. Control over the polarization state of the laser- or led-light in these applications is often needed, and many times provided by microstructure-based polarizers and wave-plates. These form-

birefringent microstructures can again be seen as a mimic of nature, since similar effects are found not only among natural crystals but also, for example, in the eye of a crustacean species [13]. Form-birefringent microstructures are discussed in several theoretical and experimental studies from recent years, mainly trying to overcome some experimental difficulties [14–31]. In this thesis, some progress is brought to this field of research.

Another topic discussed in this book is optical activity, a form of light-matter interaction which is vitally important in chemistry, biology, mineralogy, and optics [32–36]. Optical activity is a natural property of chiral or helical molecules and crystals, but it can also be achieved with many kinds of artificial chiral meta-metarials and microstructures [37–40]. Interestingly, optical activity can occur also among non-chiral microstructures when combined with specific illumination arrangements [41–43]. In this thesis, a non-chiral diffracting configuration is shown to produce optical activity much stronger than with any previously studied meta-material.

The first two chapters of this book discuss the electromagnetic theory of light, and basics of diffractive optics and polarization analysis. Comprehensive treatments of theory are not included, but rather just a brief background for the actual results of the thesis. In chapter 4, an original method for designing polarization shaping diffractive elements is introduced. The main results of the thesis include fabrication of planar micro structures with electron beam lithography, and these experimental aspects are also discussed in chapter 4. Chapter 5 briefly introduces the results, which are presented in more detail in the attached journal papers **I**–**IV**. In chapter 6, some concluding remarks are made.

2 *Electromagnetic presentation of polarized light*

Electromagnetic theory treats light as propagating oscillations of electromagnetic field. This treatment is needed for studying such phenomena as refraction, interference and diffraction. Polarization of light is a straight consequence of the vectorial nature of electromagnetic fields. Starting from the famous Maxwell's equations, one can draw mathematical expressions for some very complex physical optics. Here the depths of the theory are not covered, but still we need to go through some details that are needed for the analysis later in this thesis. This chapter is a condensed look on these parts of the electromagnetic theory.

2.1 LIGHT IN HOMOGENOUS MEDIUM

The basis of electromagnetic theory is the four differential equations named after a 19th century physicist James Clerk Maxwell [5]. These equations link together five vector quantities: electric field, magnetic field, electric displacement, magnetic induction, and the current density. They describe the interaction between light and surrounding media. Adding in also the so called constitutive relations between these quantities, one can describe the electromagnetic field with only two quantities, usually the electric field $\boldsymbol{E}$ and the magnetic field $\boldsymbol{H}$.

Any time harmonic wave in a homogenous medium is a solution of Maxwell's equations. The simplest example is a monochromatic plane wave, presented here with the aid of the electric field as a function of position $\boldsymbol{r}$ and time t.

$$\boldsymbol{E}(\boldsymbol{r},t) = \Re\{(E_x\hat{\boldsymbol{x}} + E_y\hat{\boldsymbol{y}} + E_z\hat{\boldsymbol{z}})\exp(\mathrm{i}\boldsymbol{k}\cdot\boldsymbol{r} - \mathrm{i}\omega t)\} \tag{2.1}$$

where $\boldsymbol{k}$ is the wave vector, ω is the angular frequency, and E_x, E_y, and E_z are the Cartesian complex amplitude components of the electric field. Complex valued quantities, in the form $E_j = |E_j| \exp[\mathrm{i} \arg(E_j)]$, are used since they posses both amplitude and phase information. In real life, observing the time dependency is impossible, and only a time-averaged field strength, i.e. intensity, can be detected.

Perfect plane waves do not exist in nature but they are good theoretical models. More complex fields can be presented as a superposition of plane waves with different amplitudes and wave vector components, known as the angular spectrum presentation [44]. However in this thesis, we confine to treat light as single plane waves. Although it is not altogether physically accurate, this method provides sufficient information of light interaction with microstructures.

2.2 POLARIZATION

Electric field is a vector quantity. Therefore also electromagnetic vibrations have directions of oscillation, referred to as the *polarization direction*. The term *polarized light* is used when the oscillation direction is constant, or if it changes deterministically as a function of time. The former is referred to as *linear polarization*, and the latter as *elliptical polarization*. If the time dependency is random, light is said to be *unpolarized*. *Partially polarized* light is a combination of polarized and unpolarized parts.

Different polarization states are illustrated in figure 2.1. In elliptical polarization the electric field vector draws an ellipse as a function time. An elliptical state can be defined by the polarization angle ψ and ellipticity β, as in Fig. 2.1 (d). Linear and *circular polarization* can be seen as special cases of elliptical polarization. In a linear state $\beta = 0^\circ$, and in a circular one $\beta = 45^\circ$.

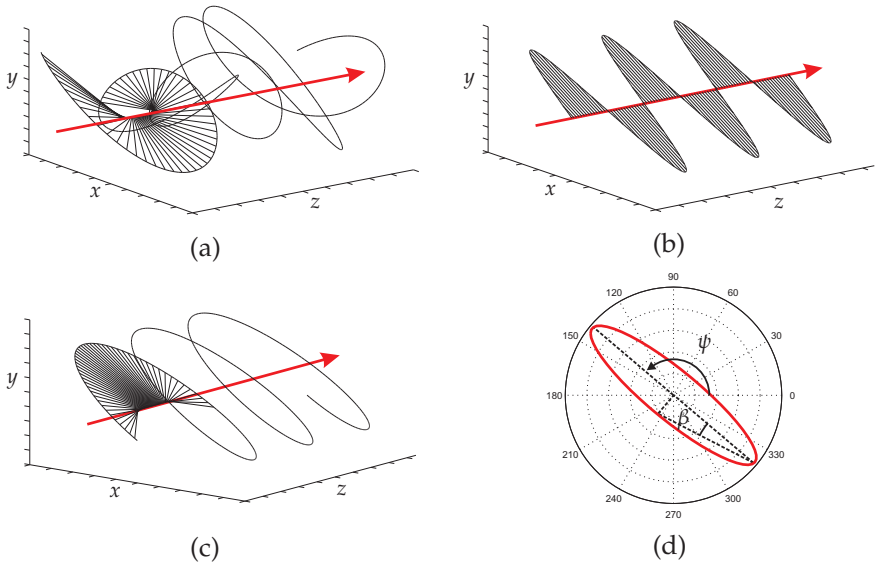

Figure 2.1: Illustrations of (a) unpolarized, (b) linearly, and (c) elliptically polarized electromagnetic oscillation. Red vector represents the propagation direction of the wave, the black lines represent the oscillating electric field vector in the x, y-plane. (d) Definition of an elliptical state by angles ψ and β.

2.2.1 Jones presentation

For a plane wave in isotropic media, Maxwell's equations impose that the electric $\boldsymbol{E}$ and magnetic field $\boldsymbol{H}$ are always perpendicular to the propagation direction, defined by $\boldsymbol{k}$, and to each other. Therefore with a proper choice of coordinate system, we can neglect the third complex amplitude component in Eq. (2.1). The remaining two components are arranged in a column vector, also known as the *Jones vector*. The two components are hereafter called the transverse electric (TE) and transverse magnetic (TM) (the definitions for TE and TM are given in section 3.1). The electric field can now be expressed as

$$\boldsymbol{E}(\boldsymbol{r}) = \begin{bmatrix} E_{\mathrm{TM}} \\ E_{\mathrm{TE}} \end{bmatrix} \exp(\mathrm{i}\boldsymbol{k}\cdot\boldsymbol{r}) = \begin{bmatrix} |E_{\mathrm{TM}}| \\ |E_{\mathrm{TE}}|\exp(\mathrm{i}\delta) \end{bmatrix} \exp(\mathrm{i}\boldsymbol{k}\cdot\boldsymbol{r}) \quad (2.2)$$

where δ is the relative phase difference $\arg(E_{\mathrm{TM}}) - \arg(E_{\mathrm{TE}})$. Note that the time dependency is ignored here for simplicity. Note also that from here on the absolute phases of the components are not relevant and we focus only on the relative phase difference. Next, let us define a normalized Jones vector as

$$\boldsymbol{J} = \frac{1}{|\boldsymbol{E}|} \begin{bmatrix} E_{\mathrm{TM}} \\ E_{\mathrm{TE}} \end{bmatrix}. \tag{2.3}$$

Normalized Jones vectors provide a enlightening way to view different polarization states. For example

$$\boldsymbol{J}_{\mathrm{TM}} = \begin{bmatrix} 1 \\ 0 \end{bmatrix} \ , \ \boldsymbol{J}_{\mathrm{TE}} = \begin{bmatrix} 0 \\ 1 \end{bmatrix} \ , \text{ and } \ \boldsymbol{J}_{\psi} = \begin{bmatrix} \cos\psi \\ \sin\psi \end{bmatrix} \tag{2.4}$$

for fields that are linearly polarized in TM-, TE-, and an arbitrary direction ψ, with respect to the TM-direction. Similarly

$$\begin{aligned} \boldsymbol{J}_{\mathrm{RCP}} &= \frac{1}{\sqrt{2}} \begin{bmatrix} 1 \\ i \end{bmatrix} \ , \ \boldsymbol{J}_{\mathrm{LCP}} = \frac{1}{\sqrt{2}} \begin{bmatrix} 1 \\ -i \end{bmatrix} \ , \\ \text{and } \ \boldsymbol{J}_{\mathrm{ell}} &= \begin{bmatrix} \cos\psi \\ \exp(\mathrm{i}\alpha)\sin\psi \end{bmatrix} \end{aligned} \tag{2.5}$$

for a right-handed (RCP) and left-handed (LCP) circular polarizations, and an arbitrary elliptical polarization (ell), where $\alpha \in [0, 2\pi]$ is some fixed phase difference.

Jones vectors are especially convenient in the analysis of light propagation through a polarization-changing element. Any deterministic non-scattering element can be portrayed as a two-by-two Jones matrix $\mathbf{M}$ of four complex valued coefficients. Propagation through the elements is simply presented as a multiplication

$$\boldsymbol{J}_{\mathrm{out}} = \mathbf{M}\boldsymbol{J}_{\mathrm{in}} = \begin{bmatrix} M_{11} & M_{12} \\ M_{21} & M_{22} \end{bmatrix} \begin{bmatrix} E_{\mathrm{TM}} \\ E_{\mathrm{TE}} \end{bmatrix}_{\mathrm{in}}. \tag{2.6}$$

It is often useful to define the Jones matrix with its eigenvectors $\boldsymbol{V}_1$, $\boldsymbol{V}_2$ and eigenvalues D_1 and D_2,

$$\mathbf{M} = D_1\boldsymbol{V}_1\boldsymbol{V}_1^\dagger + D_2\boldsymbol{V}_2\boldsymbol{V}_2^\dagger. \;\Rightarrow\; \mathbf{M}\boldsymbol{V}_j = D_j\boldsymbol{V}_j \quad , \quad j = 1,2 \quad , \tag{2.7}$$

where † denotes Hermitian conjugate. The vectors $\boldsymbol{V}_1$ and $\boldsymbol{V}_2$ represent certain polarization states, called the *eigenpolarizations* of the element, which go through the element unchanged. Any third Jones vector can be presented as a linear combination of the two eigenstates, and the eigenvalues describe the scaling and phase delay of the eigenstates passing through the element. Thus the eigenvectors and values together describe the polarization changes inside the element.

2.2.2 Stokes parameters and Poincare sphere

Another way for presenting the polarization state are the Stokes parameters, defined as

$$\begin{aligned} S_0 &= |E_{\mathrm{TM}}|^2 + |E_{\mathrm{TE}}|^2 \quad & S_1 &= |E_{\mathrm{TM}}|^2 - |E_{\mathrm{TE}}|^2 \\ S_2 &= 2\Re\{E_{\mathrm{TM}}^* E_{\mathrm{TE}}\} & S_3 &= 2\Im\{E_{\mathrm{TM}}^* E_{\mathrm{TE}}\}. \end{aligned} \tag{2.8}$$

We also define the normalized Stokes parameters $s_j = S_j/S_0$, where $j = 1,2,3$. It is evident that $|s_j| \leq 1$, and with a closer look one finds also that $s_1^2 + s_2^2 + s_3^2 = 1$. Therefore, by creating a Cartesian base formed by unit vectors $\hat{\boldsymbol{s}}_1, \hat{\boldsymbol{s}}_2$, and $\hat{\boldsymbol{s}}_3$, the normalized Stokes parameters define the surface of a sphere,

$$\boldsymbol{p} = s_1\hat{\boldsymbol{s}}_1 + s_2\hat{\boldsymbol{s}}_2 + s_3\hat{\boldsymbol{s}}_3. \tag{2.9}$$

This so-called Poincare Sphere, depicted in Fig.2.2, provides a nice visual insight on different polarization states. Each point on the surface describes a certain (fully polarized) polarization state, and thus each state is specified by spherical coordinates ϑ_p and φ_p,

$$\vartheta_p = \arccos(s_3/|\boldsymbol{p}|)$$
$$\varphi_p = \arctan(s_2/s_1). \tag{2.10}$$

The poles of the sphere correspond to circular polarizations ($\vartheta_p = 0°$ for right-hand, and $\vartheta_p = 180°$ for left-hand). Linearly polarized states lie on the equator ($\vartheta_p = 90°$). The rest of the surface represents different elliptical states. Points inside the sphere, i.e. when $|\boldsymbol{p}| < 1$, represent partially polarized states.

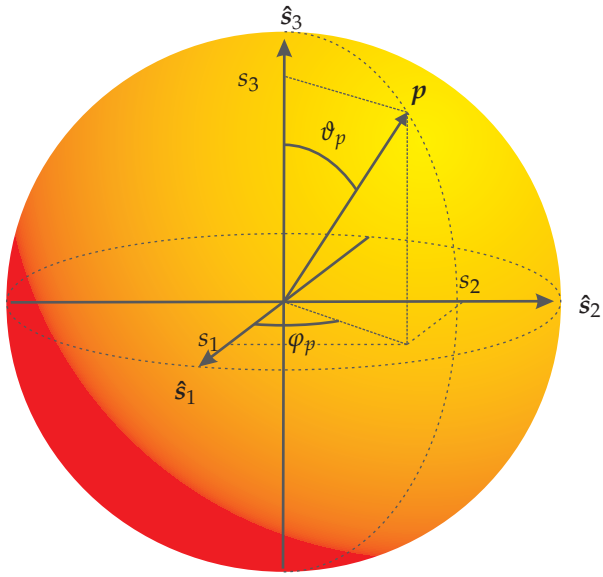

Figure 2.2: The Poincare sphere. Polarization state with Stokes parameters s_1, s_2, and s_3 is presented as a point p on the surface of the sphere.

3 Diffractive optical elements

The center of this study is in the interaction between light and periodic structures. In this chapter we will look at the theoretical principles needed to analyze this interaction. The electric field before, after, and inside of a periodic surface relief structure is solved using the rigorous Fourier Modal Method [45, 46]. Again, all the depths of the method are not covered here. However, specific attention is payed to the so called S-matrices, a feature of many rigorous methods which has been especially utilized in this work.

3.1 GRATING DIFFRACTION

Let us consider the situation illustrated in Fig. 3.1. A plane wave is incident on a periodically modulated surface characterized by periods d_x and d_y. The direction of the incidence is specified by angles θ and ϕ. The term conical incidence is used when $\phi \neq 0$. The plane defined by the wave vector $\boldsymbol{k}_0$ and surface normal $\hat{\boldsymbol{z}}$ is referred to as the plane of propagation. The aforementioned polarization components TM and TE are defined such that TM is parallel, and TE is perpendicular to the plane of propagation.

The permittivity profile of the modulated layer is

$$\epsilon(x, y, z) = \epsilon(x + d_x, y + d_y, z). \tag{3.1}$$

The periodicity of the modulated layer entails that the field in regions I and III is pseudoperiodic. In other words any Cartesian component of the field obeys the so-called Floquet–Bloch condition

$$U(x + d_x, y + d_y, z) = U(x, y, z) \exp[\mathrm{i}(k_{0x} d_x + k_{0y} d_y)] \,, \tag{3.2}$$

where k_{0x} and k_{0y} are the x- and y-components of the wave vector of the incident light. From Eq. (3.2) it follows that for the transmitted

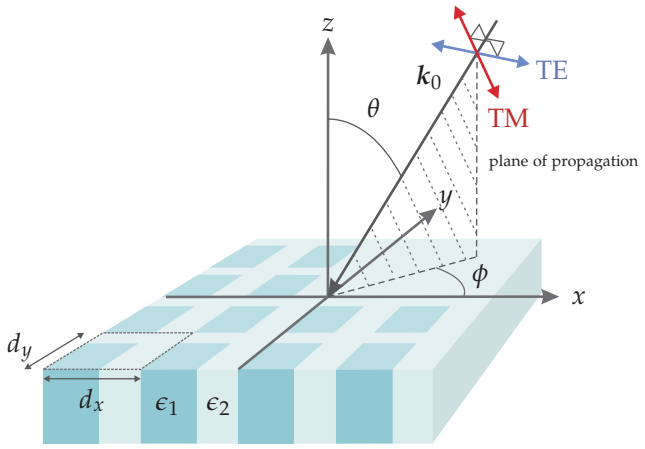

Figure 3.1: Conical incidence on a two dimensionally periodic surface.

and reflected fields k_x and k_y can only have discrete values. Consequently, we obtain the well known grating equation, presented here for the transversal part (k_x and k_y) in vector form

$$\boldsymbol{k}_{mn} = \boldsymbol{k}_0 + m\boldsymbol{g}_x + n\boldsymbol{g}_y \,, \tag{3.3}$$

where $\boldsymbol{g}_x = 2\pi/d_x\hat{\boldsymbol{x}}$ and $\boldsymbol{g}_y = 2\pi/d_y\hat{\boldsymbol{y}}$ are the grating vectors. The subscripts m, n correspond to a 2D-array of diffraction orders, as depicted in Fig. 3.2. Each diffraction order is seen as an individual plane wave. The total field is a discrete superposition of these plane waves.

3.2 FOURIER MODAL METHOD

The wave vectors of the diffraction orders are analytically given by the grating equation (3.3). The complex amplitudes, however, can only be solved with a suitable numerical method, save for a few special cases. Several such methods exist [47]. In this work, a method called the Fourier Modal Method (FMM) is used. FMM is based on presenting the field inside the grating layer, as well as the permittivity distribution of the layer, as Fourier series [46, 48].

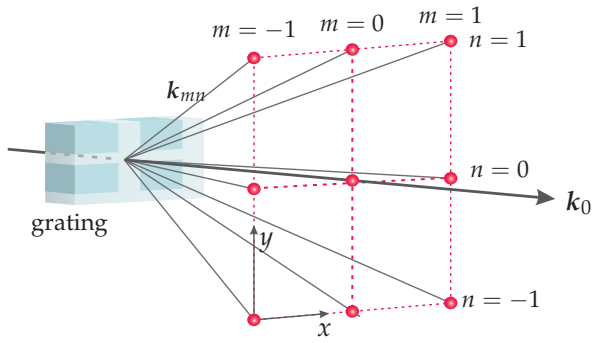

Figure 3.2: A two-dimensionally periodic grating produces a grid array of diffraction orders (m, n)*, with wave vectors* $\mathbf{k}_{mn}$*.*

The field inside the grating is expressed as a sum of a finite amount of forward and backward propagating grating modes. The modes themselves can be presented as superpositions of plane-wave components, which propagate inside the grating layer in different directions. The fields outside the grating region are expressed as a sum of propagating and evanescent diffraction orders, analogous to the plane wave components inside the grating. The complex amplitudes of the diffraction orders are solved by matching them to the field inside the grating with the boundary conditions of Maxwell's equations and with the so called *S-matrix algorithm*. [46, 49–51]

Consider a grating region that is split into n layers. In each layer we have a set of upward and downward propagating eigenmodes, whose complex amplitudes are arranged in column vectors $\mathbf{u}$ (upward) and $\mathbf{d}$ (downward). For each two adjacent layers $0 < p < n$ and $p + 1$ we can form relations that connect the modes $\mathbf{u}_{p+1}$ and $\mathbf{d}_p$ to $\mathbf{u}_p$ and $\mathbf{d}_{p+1}$. In other words, the modes outgoing from, and incoming to the layer interface. The S-matrix algorithm employs a set of recursion formulas to generate a stack S-matrix from these individual interface relations. This stack S-matrix then connects the fields in layer 0 (incident medium) and layer $n + 1$ (output medium):

$$\begin{bmatrix} \boldsymbol{u}_{n+1} \\ \boldsymbol{d}_0 \end{bmatrix} = \mathbf{S}_n \begin{bmatrix} \boldsymbol{u}_0 \\ \boldsymbol{d}_{n+1} \end{bmatrix} = \begin{bmatrix} T^n_{uu} & R^n_{ud} \\ R^n_{du} & T^n_{dd} \end{bmatrix} \begin{bmatrix} \boldsymbol{u}_0 \\ \boldsymbol{d}_{n+1} \end{bmatrix} . \tag{3.4}$$

If we assume that there are no sources after the grating (medium $n+1$) we have $\boldsymbol{d}_{n+1} = \mathbf{0}$. Consequently we can write for the complex amplitudes of the transmitted $\boldsymbol{t}_{mn}$ and reflected $\boldsymbol{r}_{mn}$ diffraction orders:

$$\begin{aligned} \boldsymbol{t}_{\mathrm{mn}} &= \boldsymbol{u}_{n+1} = T^n_{\mathrm{uu}} \boldsymbol{u}_0 \\ \boldsymbol{r}_{\mathrm{mn}} &= \boldsymbol{d}_0 = R^n_{\mathrm{du}} \boldsymbol{u}_0 \ , \end{aligned} \tag{3.5}$$

where T^n_{uu} and R^n_{du} are submatrices of the stack S-matrix. [46,49–51]

3.3 POLARIZATION STATE MANIPULATION

The basic principle of polarization state manipulation is simplified in Fig. 3.3. Incident light, with a Jones vector J_{in}, interacts with a body of anisotropic medium. Either the reflected or transmitted light, with a changed Jones vector J_{out}, is observed. Three different well-established physical principles for such polarization state changing interaction are presented in this section. Each principle exists also in other kinds of media, but here we present them as related to planar microstructures, the so-called *subwavelength*, or *zeroth-order* gratings. When the period of a diffraction grating is below the certain threshold value $d_{\mathrm{swl}} \simeq \lambda$, the diffracted field consists of only one propagating Fourier component. In other words, only the zeroth diffraction order exists in the far-field.

3.3.1 Wire-grid polarizers

A wire-grid polarizer (WGP) is a periodic structure consisting of metallic wires, so to speak. Since light is basically an oscillating electromagnetic force, incidence on a metallic surface causes electron movement in the direction of the electric field, due to the

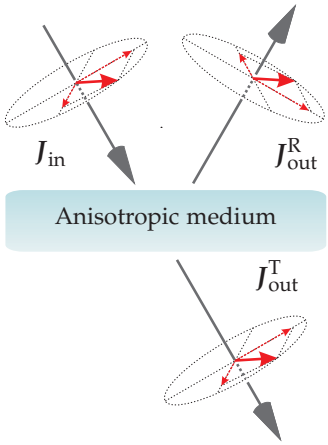

Figure 3.3: The principle for polarization state manipulation.

Lorentz interaction [52]. The effect is widely used in crossed structures acting as spectral filters [53,54]. In WGP however, the electron movement is possible only in the direction of the wires. Therefore the induction strength is varied largely depending on the electric field direction. Let us say we define the light polarized parallel to the wires as TE-component, and perpendicular to the wires as TM-component. In a perfect WGP, TM-component is transmitted while TE-component is reflected and absorbed, due to the induction. WGP is an ancient type of a device, first tests were done already in 1888 with radio waves [55], near-infrared polarizers were realized in the 1960s [56], and more recent fabrication techniques have enabled WGPs for the visible spectrum [57–63]. Some recently studied wire-grids utilize guided-mode or plasmon resonances to get enhanced, or totally new kinds of polarization selectivity [64,65].

3.3.2 Linear birefringence

Let us next consider a transparent crystal material, with principal axes $\boldsymbol{x}$, $\boldsymbol{y}$, and $\boldsymbol{z}$. The permittivity of the material is defined separately for each crystallographic direction, as ϵ_x, ϵ_y, and ϵ_z. If we

have, for example, $\epsilon_x \neq \epsilon_y = \epsilon_z$ the material is said to be *uniaxially anisotropic*, and refractive index depends on the electric field direction [52]. There are two distinct polarization states, the *eigenpolarizations* of the material, which go through the element unchanged, but experience different amplitude and phase modulation. These differences are known as *dichroism* (amplitude) and *birefringence* (phase). Since any other polarization state can be decomposed into a combination of the eigenstates, the optical behavior of the element can be described with the eigenstates and their corresponding *complex amplitude coefficients*.

Subwavelength grating structures can be used for mimicking the anisotropicity of natural crystals (such as calcite). Figure 3.4 presents a linear (one-dimensionally periodic) subwavelength grating, and normally incident light. The structure has obvious reflection symmetry in the (x,y)-plane. Symmetry axes are shown in the figure with dashed lines. The eigenstates of such structure are linear polarizations in x- and y-directions, i.e. parallel and perpendicular to the symmetry axes [66]. When put in the Jones formalism (see section 2.2.1), the grating is represented by a Jones Matrix $\mathbf{M}$ with normalized eigenvectors $\boldsymbol{V}_1$ and $\boldsymbol{V}_2$, and eigenvalues d_1 and d_2:

$$\boldsymbol{V}_1 = \begin{bmatrix} 1 \\ 0 \end{bmatrix} , \; \boldsymbol{V}_2 = \begin{bmatrix} 0 \\ 1 \end{bmatrix} , \; d_1 = A_x e^{\mathrm{i}\alpha_x} , \text{ and } d_2 = A_y e^{\mathrm{i}\alpha_y} , \quad (3.6)$$

where A_x and A_y define the amplitude modulation, and α_x and α_y represent the phase delays of the eigenstates. If we have $A_x \neq A_y$, the element is said to be linearly dichroic, and if $\alpha_x \neq \alpha_y$, linearly *form-birefringent*. By designing an element with $A_x = A_y$, and $\Delta\alpha = \alpha_x - \alpha_y = \pi$, or $\Delta\alpha = \pi/2$, we obtain a first-order half-wave, or quarter-wave plate, with fast- and slow-axis parallel and perpendicular to the grating vector, respectively. Half-wave plate flips the incoming linear polarization around the slow-axis, while a quarter-wave plate (in correct azimuthal orientation) turns it into circular polarization.

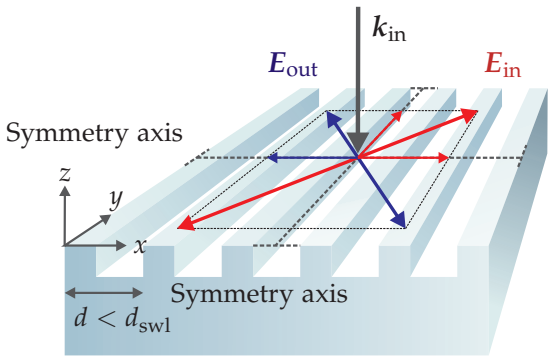

Figure 3.4: A form-birefringent grating element, with grating thickness designed for half-wave retardation.

The problem with waveplates made of natural crystals is the few-millimeter thickness of the elements, which prevents their integration into micro-optical systems. Therefore, form-birefringent wave plates have inspired some research in the last decade. Studied elements include both metallic and dielectric structures, used either in direct transmission [20], or in reflection [22,23,67]. More detailed survey of these studies is presented in the introduction of paper I. Shortly, the problem with (lossless) dielectric half-wave plates has been the high aspect ratios (grating thickness-to-period ratio) required for the half-wave retardation. Studies of quarter-wave plates have often reached achromatic behaviour [24–26]. In most recent studies, phase retardation has been produced or enhanced also with plasmonic and waveguide resonances [21,28,68,69].

3.3.3 Circular birefringence

Circular birefringence is a principle associated with chiral materials or structures. In general, a single molecule or the unit cell of a crystal material is chiral when it possesses no reflection symmetry [33]. Same principle can be applied also to periodic microstructures. Figure 3.5 presents a crossed (two-dimensionally periodic) grating structure, where the unit cell consists of a gammadion shape relief. The unit cell has no reflection symmetry, but instead a four-fold

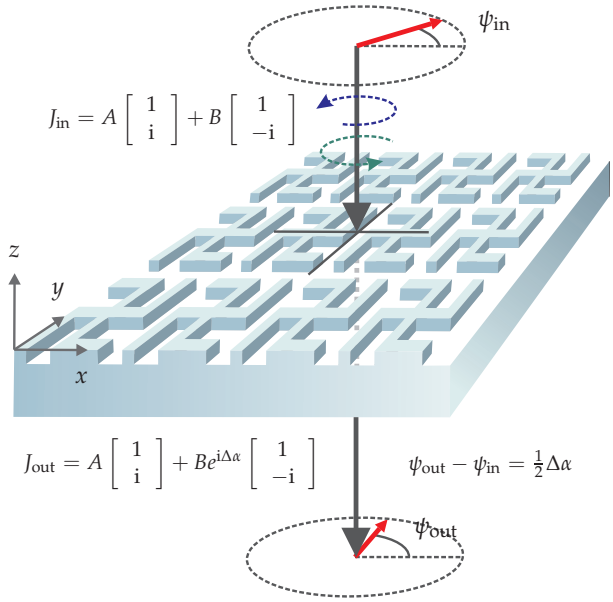

Figure 3.5: Example of a chiral grating structure. Input linear polarization ψ_{in} is rotated to ψ_{out} in the output, due to circular birefringence.

rotational symmetry. The eigenstates of such structures are always right- and left-handed circular polarizations [66]. In circular birefringence, similarly to linear birefringence, the refractive indices for the two eigenstates are different.

Any linear polarization $\boldsymbol{J}$ can be decomposed into a combination of RCP and LCP (see eq. (2.5))

$$\boldsymbol{J} = |A|e^{\text{i}\alpha_{\text{rcp}}} \begin{bmatrix} 1 \\ \text{i} \end{bmatrix} + |B|e^{\text{i}\alpha_{\text{lcp}}} \begin{bmatrix} 1 \\ -\text{i} \end{bmatrix} \tag{3.7}$$

such that $|A| = |B|$, and $\alpha_{\text{rcp}} - \alpha_{\text{lcp}} = 2\psi$ defines the polarization angle ψ. Propagation through a circularly birefringent element causes additional phase difference $\Delta\alpha$, and the polarization direction is rotated by $\Delta\psi = \Delta\alpha/2$. In other words, the rotation is the same for all input polarizations, unlike in a half-wave plate where the rotation depends on the angle difference between the input polarization and

the eigenstates. The rotation in chiral media is often referred to as *optical activity*. Difference in the transmission of the RCP and LCP eigenstates is called *circular dichroism* [33,70–72]

The physical explanation of the rotation is said to be cross-excitation of electric and magnetic dipoles by the incident electric and magnetic oscillations [73,74]. Optical activity of artificial chiral structures has been extensively studied in the recent past, including bi-layer split rings and crosses [75–78], planar metallic [79–82] and dielectric structures [38,40,83–85]. Another heap of articles has been published about artificial circular dichroism [86–88].

Most of the studied structures are *intrinsically* chiral, meaning that the chirality comes directly from the unit cell shape (as in Fig. 3.5). However, it has been shown that optical activity occurs also with structures where non-chiral unit cells are arranged in a chiral lattice. This form has been labeled *structural* chirality [89]. In addition, some studies with metallic structures have displayed a third form, labeled *extrinsic* chirality. Here, both the unit cell and the lattice are non-chiral, but the illumination setup is chiral, in the sense that the input and output wave vectors and the so called polarity vector of the structure define a three vector system with a certain handedness [41–43,90].

4 Grating design and fabrication

In this chapter we shall look at various methods and processes that are needed to change a polarization manipulating element from an idea into an actual piece of glass. The first section presents the method for simple analysis of polarization state changes in non-zeroth diffraction orders. The method is presented in more detail in paper IV. A short description of the used lithographical fabrication methods, with special attention on slanted etching, is found in the following section.

4.1 EIGENPOLARIZATION-ANALYSIS FOR DIFFRACTING ELEMENTS

As mentioned above, polarization conversions in light-matter interactions can be analyzed with the Jones algebra (section 2.2.1), taken that we know the eigenstates and their complex amplitude coefficients. In principle, this simple method applies to any polarization element, be it natural or artificial, linear or circular, and dichroic or birefringent.

There are comprehensive studies about the eigenpolarization-analysis of bulk anisotropic media [91, 92]. Recently, also periodic metamaterials have been studied, but only the case of direct transmission with normal incidence was tackled [66]. It has also been found that with special incidence mountings, also geometrically non-chiral structures can exhibit circular eigenstates [41–43]. Hence, there is need for a method of eigenpolarization-analysis of periodic (also diffracting) structures in arbitrary incidence mounting, and also including any non-zeroth diffraction order as the output.

Our goal in paper **IV** was to construct a numerical method for

defining the eigenpolarizations and their eigenvalues for an arbitrary diffraction order from any crossed grating using oblique incidence. The logic of the method is simple. Three separate Cartesian coordinate bases are created: a global system $C_0 = (x, y, z)$ where x- and y-axes are aligned with the grating vectors, and two local systems $C_{\text{in}} = (\theta, \phi, k)_{\text{in}}$ and $C_{\text{out}} = (\theta, \phi, k)_{\text{out}}$, related to the incident and the diffracted wave-vectors as illustrated in figure 4.1.

Incident Jones vector is presented in C_{in} and a coordinate transform $\mathbf{T}_{\text{in}} : C_{\text{in}} \rightarrow C_0$ is performed to present the input field in (x, y, z)-basis (requirement of Fourier modal method). With FMM we obtain the submatrices $\mathbf{T}^n_{\text{uu}}$ and $\mathbf{R}^n_{\text{du}}$ of the structure S-matrix with the designed number of Fourier components [see eq. (3.5)]. The coefficients in $\mathbf{T}^n_{\text{uu}}$ and $\mathbf{R}^n_{\text{du}}$ are related to x- and y-components of the field for each plane-wave component. We are interested in the coefficients that connect the fields of the input component $(0, 0)$ and the transmitted or reflected output components (m, n). We arrange these coefficients into matrices $\mathbf{S}^{(\text{t})}_{mn}$ and $\mathbf{S}^{(\text{r})}_{mn}$.

$$\mathbf{S}^{(\text{t})}_{mn} = \begin{bmatrix} s^{(\text{t})}_{xx} & s^{(\text{t})}_{xy} \\ s^{(\text{t})}_{yx} & s^{(\text{t})}_{yy} \end{bmatrix} \quad \mathbf{S}^{(\text{r})}_{mn} = \begin{bmatrix} s^{(\text{r})}_{xx} & s^{(\text{r})}_{xy} \\ s^{(\text{r})}_{yx} & s^{(\text{r})}_{yy} \end{bmatrix} , \tag{4.1}$$

If for example the transmitted $(-1, 0)$th order is observed, we use the matrix $\mathbf{S}^{(\text{t})}_{-1,0}$ to obtain the output field in global coordinates. Then, a second coordinate transform $\mathbf{T}_{\text{out}} : C_0 \rightarrow C_{\text{out}}$ is performed, to present the output field in the local system of the $(-1, 0)$th order.

The coordinate transforms are needed if we wish to compare the Jones vectors of the input and output beams. Now, we can define a Jones matrix M_{mn} that describes the possible polarization conversion in the interaction as

$$\begin{bmatrix} E_{\text{TM}} \\ E_{\text{TE}} \end{bmatrix}^{(\text{t,r})}_{mn} = \mathbf{M}^{(\text{t,r})}_{mn} \begin{bmatrix} E_{\text{TM}} \\ E_{\text{TE}} \end{bmatrix}_{\text{in}} , \text{ where} \tag{4.2}$$

$$\mathbf{M}^{(\text{t,r})}_{mn} = \mathbf{T}_{\text{out}} \mathbf{S}^{(\text{t,r})}_{mn} \mathbf{T}_{\text{in}} . \tag{4.3}$$

The eigenvectors of $\mathbf{M}_{mn}$ are Jones vectors representing the eigenpolarizations of this particular interaction. It must be emphasized that the eigenpolarizations may depend also on the geometry formed by k_{in} and k_{out}, and not only the symmetry of the grating, as it is demonstrated in paper **IV**. The eigenvalues of $\mathbf{M}_{mn}$ describe the possible dichroism and birefringence-like effects between the eigenpolarizations. Therefore, we can easily optimize the grating profile parameters for polarizer-, waveplate-, or rotator-type effects, with a merit function consisting only of the eigenvectors and eigenvalues of $\mathbf{M}_{mn}$.

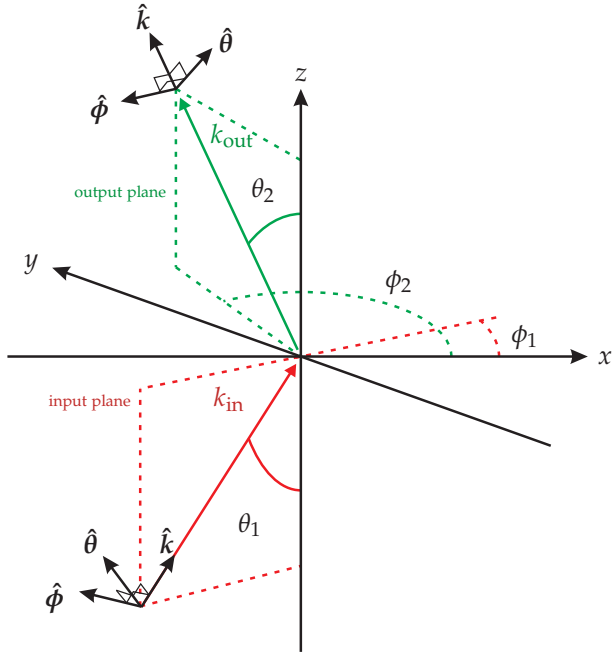

Figure 4.1: Illustration of the local coordinate systems of the input (red) and output (green) beams.

4.2 FABRICATION OF SLANTED GRATINGS

There are many types of optical structures that are collectively referred to as gratings, and many ways for their categorization. The

elements to be discussed later in this thesis belong to the class of surface-relief structures, where separate families are formed by metallic and dielectric structures, in which different species can be separated by their profile type (single- or multilayer; binary or continuous). In this thesis, special attention is paid to a species called *slanted gratings*.

Figure 4.2 illustrates the simple difference between a standard binary, and a slanted binary grating profile. A slanted grating is basically a binary grating with its vertical axis skewed to an angle Θ. Since slanted gratings hold an asymmetrical quality, they have been used for asymmetrical optical functions such as unidirectional surface plasmon excitation and waveguide in-coupling [93–96]. The numerical modeling of a slanted structure is carried out using FMM with the modification of arbitrarily oriented coordinate axes, presented in [51].

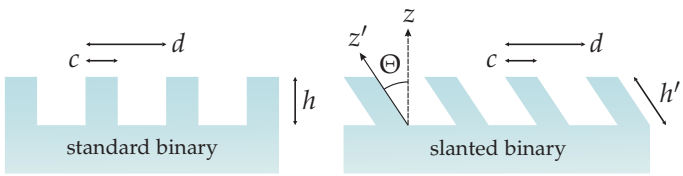

Figure 4.2: The profile shapes of a standard binary surface relief grating, and a slanted counterpart.

The fabrication of surface relief gratings in general is a large collection of different lithographic processes and techniques. In this section the processes used in the experimental work of papers **II** and **III** are introduced. The key-process in this line of work is electron beam lithography (EBL) which enables us to realize the rather small lateral dimensions of subwavelength structures. In the process steps following EBL, the created lateral pattern is only transferred from one material to another. Figure 4.3 illustrates the flow of processes. Two separate roads that lead to similar final results were used in this study.

4.2.1 Electron beam lithography

In the electron beam lithography system, a focused beam of accelerated thermal electrons is inflicted upon a sensitive material, *resist*, where changes in the polymeric structure are triggered by absorbed electrons. The beam draws the desired pattern into the resist layer (few tens to few hundred nanometers thick) in very high resolution. Depending on the type of resist, the exposed areas become either more soluble (positive resist) or insoluble (negative) in a specific developer solution. Therefore, after the development we have a relief resist structure on the substrate.

From a variety of different e-beam resists, two different positive resists have been used for this study: AR-P 661 (Allresist GmbH) and ZEP 7000-22 (Zeon Corporation). The exposures were carried out with Vistec EBPG 5000+ES HR e-beam system, which has a 100 kV acceleration voltage and a minimum spot size less than 2.5 nanometers.

4.2.2 Chromium mask fabrication

The resist grating is rarely the final structure, and in most cases the goal is to etch the grating structure into the substrate. Reactive ion etching (RIE) is a process in which bombardment of ions or free radicals removes material from the sample surface. The sample is placed in a low-pressure chamber, between two electrodes. Process-specific etching gases are used for creating a chamber atmosphere with accurately controllable gas pressure, and chemical composition.

The gas is brought to plasma phase with an electric field oscillating in a radio frequency (RF) between the electrodes. The electrons stripped from the gas atoms build up a negative charge on the sample surface, which causes the positive ions to accelerate towards it. The ions react with the surface, resulting in physical (anisotropic) and chemical etching (isotropic) of the material. Various process parameters can be adjusted to control the process, most significantly the RF-generator power and chamber pressure. [97, 98]

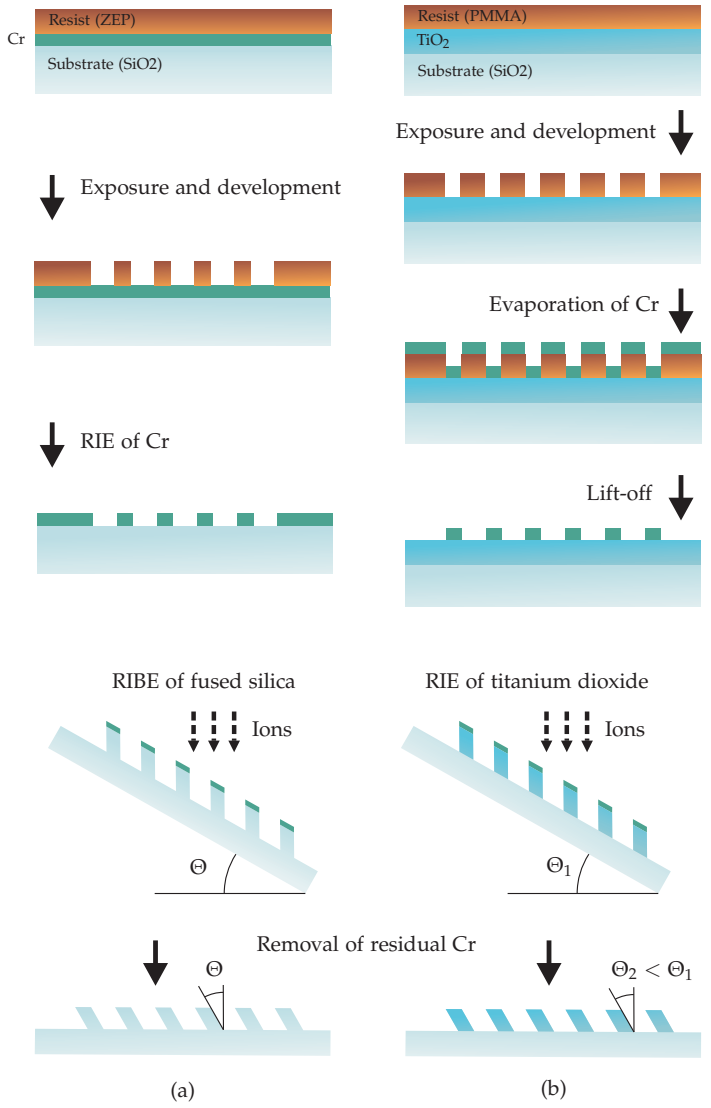

*Figure 4.3: Two fabrications schemes for slanted structures, (a) used in paper **III**, and (b) used in paper **IV**.*

Any relief structure on top of the sample acts as an etching mask for the layer below it, exposing only certain areas for erosion. Therefore, the lateral pattern of the mask is transferred to the layer below.

Small deformations of the ideal straight-wall profile occur due to various physical and chemical effects inside the chamber [99, 100]. The erosion speeds of different materials under the same process gases are unequal, and metals such as chromium are great mask materials for the etching of dielectrics such as fused silica (SiO_2) and titanium dioxide (TiO_2). Chromium mask itself can be etched with a chlorine-based process using the resist pattern as a mask. This method was used in paper **III**.

Another way for obtaining the chromium mask, called lift-off, was used in paper **II**. Lift-off is a process where a layer of metal is deposited on top of (and in the grooves of) a resist grating, followed by a chemical removal of the resist, leaving only the metal in the grooves attached to the substrate (see Fig. 4.3). A good choice for a lift-off resist is a Polymethyl metacrylate (PMMA), such as the AR-P 661 used in this study. PMMA is removed by soaking in acetone. It must be noted, that RIE is generally the superior method compared to lift-off.

4.2.3 Slanted etching

After obtaining the chromium mask with above mentioned methods, the next step is the actual slanted dry etching of the substrate. A suitable method for this is *reactive ion beam etching* (RIBE). In RIBE, the ions are created in a separate source and then accelerated onto the sample surface. The sample can be tilted to change the angle of incidence of the ion bombardment. Compared to RIE, this is an advantage that enables proper slanted etching. The SiO_2 structures in paper **III** were etched with Oxford Plasma Technology Ionfab 300 Plus RIBE machine, using an Ar/ChF_3 atmosphere.

However, also RIE is capable of slanted etching, at least to some extent. For the slanted TiO_2 structures in paper **II**, we used a SF6/Ar RIE process with low gas pressure (20 mTorr) and high RF-generator power (300 W). These settings emphasize the physical etching over the chemical one and, therefore, it is possible to achieve a small tilt in the etching direction. In our case, tilting the

sample to approximately 60 degrees produced a slanted etching direction of around 30 degrees.

5 Main results

This chapter introduces the theoretical and experimental results in papers **I–III**. The contents of paper **IV** were discussed already in the previous chapter. In addition, an unpublished theoretical result concerning optical activity is presented in section 5.4. In all presented results, dielectric microstructures are used for efficient polarization state manipulation for monochromatic light.

5.1 POLARIZATION CONVERSION IN TOTAL INTERNAL REFLECTION

The main idea of paper **I** is a thorough theoretical examination of the half-wave retardation, or in other words, TE to TM -polarization conversion, occurring in the reflected zeroth order in a total internal reflection arrangement. Both metallic and dielectric gratings were studied. We noted that studies on the same subject had already been published [22, 23, 67]. The novelty we intended to bring was the use of FMM with conical incidence, and careful optimization of the structures for the best possible fabrication feasibility. With this type of elements the best fabrication feasibility usually follows from the lowest possible grating thickness. The studied elements were linear, rectangular profile binary gratings made of gold, silver, aluminium, and titanium dioxide, on top of a fused silica substrate. The grating period was fixed to 250 nm, and the angle of incidence to 45 degrees. Refractive index data for the metals was taken from [101]. In all cases, HeNe light with $\lambda = 633$ nm was used.

The outcome of the material comparison was that, from the three metals, a gold grating would produce the half-wave effect with the highest reflectance (82.23%). The thickness of the gold structure would be 283 nm. However, dielectrics proved to be much more interesting. A dielectric grating with refractive index 2.0 would require 630 nm thickness for the half-wave retardation,

while a refractive index of 2.3 would reduce the requirement to 405 nm. The refractive index of vacuum deposited titanium dioxide is usually between these two values. It is clear that due to the total internal reflection setup and the absence of absorption, a 100% reflectance is associated with the dielectric element. Based on the design results, a titanium dioxide grating was lithographically fabricated and measured, and the outcome was published in [2].

5.2 PHASE SHIFT BY WAVEGUIDING

In paper II, we intended to overcome the difficulties related to half-wave retardation in direct transmission. A traditional form-birefringent element made with high-refractive-index material requires large grating thicknesses that are not suitable for reasonable fabrication [20].

Our invention is based on a linear slanted structure in which the behavior of TM- and TE-polarized input light is fundamentally different. Figure 5.1 presents the principle. In general, the structure with a period small enough acts as true effective medium. Then again, with periods in the order of the wavelength, the structure may act as an array of slanted pillar waveguides. We found that with a certain period between these regions, TE-polarized light experiences the "waveguide-structure" while TM-polarized light still sees an uniform layer.

When light is coupled along the pillars, the optical path and,

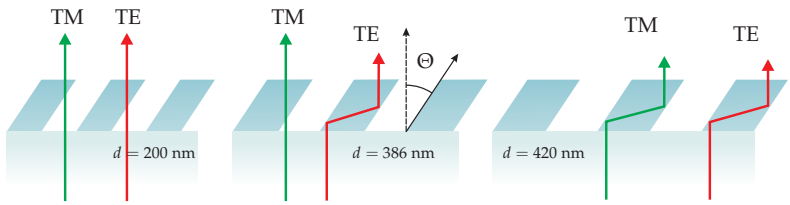

Figure 5.1: A simplified schematic of selective coupling in a linear slanted grating. A large phase difference between TM- and TM-polarizations arise with a correctly adjusted period ($d = 386$ nm in this example design for $\lambda = 633$ nm).

consequently, also the phase delay are increased. The increase may be further affected by resonance effects, which are common inside structures with period in the order of the wavelength. The situation where the orthogonal polarizations behave differently ($d = 386$ nm for $\lambda = 633$ nm wavelength) can be used to obtain large phase retardation. This effect can not be called form-birefringence, but instead a new phenomenon of its own.

The phase retardation occurring in the slanted structure can be adjusted to an exactly half-wave shift between TE- and TM-components. In Table 1 of paper **II**, four different designs based on this type of structure are presented. The most significant design is the one on the second row, where the grating thickness is merely 262 nm with a 400 nm period. The design on the third row is for an experimental test piece, with a smaller slant angle $\Theta = 33^\circ$ but higher thickness $h = 648$ nm. An element based on this design was fabricated and optically tested. The resulting structure was not totally in agreement with the design, but it still produced a 177 degrees (designed value 180°) phase shift measured with a HeNe laser and the so called quarter-wave plate method [29]. The agreement between numerical calculations and experiments was verified by re-running the calculations with the actual grating profile shape. Figure 5.2 presents a cross section scanning electron microscope image of the element. The slanted profile was divided into 32 binary layers, and the layered profile was used in the numerical verification with FMM.

The refractive indices of our in-house thermally deposited TiO_2 layers are varied slightly around $n \approx 1.99$ (for $\lambda = 633$ nm) between experiments, according to ellipsometer measurements. The variation of both the exact value of the refractive index and the error margin of the grating thickness measurement from the SEM image must be taken into account in the comparison of numerical and experimental data. With these variations, the numerical calculation with the layered profile (Fig. 5.2) resulted in a phase shift similar to the measured 177 degrees, and the transmittances of TE- and TM-polarizations were nearly equal.

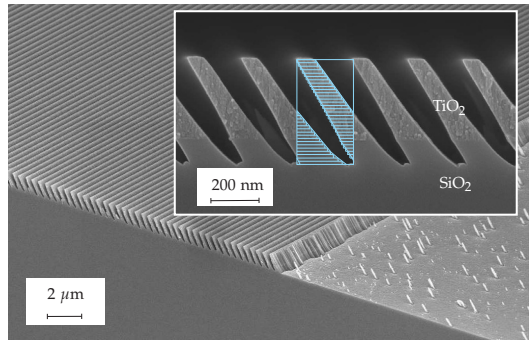

*Figure 5.2: A cross section SEM image of the fabricated prototype from paper **II**.*

5.3 HALF-WAVE EFFECT IN DIFFRACTED LIGHT

The design method presented in Section 4.1 enables optimization of complex 3-D structures for polarization effects in any given diffraction order. Two results found with this method are presented in this section and in the next one. Both effects occur with oblique incidence on a linear grating made of anisotropic material, with specifically rotated anisotropy axes, as presented in Fig. 5.3 (a). In practise, such structure can be mimicked with a two dimensionally periodic slanted profile grating. In both of the following results, the mutual geometry of the grating and input and output wave-vectors produces an interaction with a rather unexpected Jones matrix operator.

The first result is presented in paper **III**. Let us consider that guided light, inside a slab lightguide, is incident on a crossed grating on top of the lightguide. The grating geometry is as depicted in Fig. 5.3 (b). The period in the x-direction is fixed to the 2nd order Littrow condition, i.e. the -2nd reflected order propagates exactly in the opposite direction as the incident wave. The grating profile in the y-direction is slanted with an angle Θ, and the grating period d_y is well below the wavelength. Therefore, the structure is basically a linear grating in the x-direction consisting of stripes of air and anisotropic uniaxial material with crystal axes x, y', and z', and permittivity tensor $\tilde{\epsilon}$:

$$\tilde{\epsilon} = \mathbf{R}_{x,\Theta} \begin{bmatrix} \epsilon_\mathrm{o} & 0 & 0 \\ 0 & \epsilon_\mathrm{e} & 0 \\ 0 & 0 & \epsilon_\mathrm{o} \end{bmatrix} \mathbf{R}_{x,\Theta}^T \quad , \quad \mathbf{R}_{x,\Theta} = \begin{bmatrix} 1 & 0 & 0 \\ 0 & \cos\Theta & -\sin\Theta \\ 0 & \sin\Theta & \cos\Theta \end{bmatrix}$$

$$\tilde{\epsilon} = \begin{bmatrix} \epsilon_\mathrm{o} & 0 & 0 \\ 0 & \epsilon_\mathrm{e}\cos^2\Theta + \epsilon_\mathrm{o}\sin^2\Theta & (\epsilon_\mathrm{e} - \epsilon_\mathrm{o})\sin\Theta\cos\Theta \\ 0 & (\epsilon_\mathrm{e} - \epsilon_\mathrm{o})\sin\Theta\cos\Theta & \epsilon_\mathrm{e}\sin^2\Theta + \epsilon_\mathrm{o}\cos^2\Theta \end{bmatrix}. \tag{5.1}$$

Let us next look at the field inside the grating layer. With careful optimization, we obtain a structure in which the field consists practically of only two orthogonally polarized plane wave components: The 0th order component, propagating roughly parallel to the incident wave, and the -2nd order components, which propagates roughly opposite to the incident wave. The amplitudes and polarizations of the plane-wave components can be excerpted from FMM calculations.

As is presented in Fig. 3 of paper **III**, it is found that, imme-

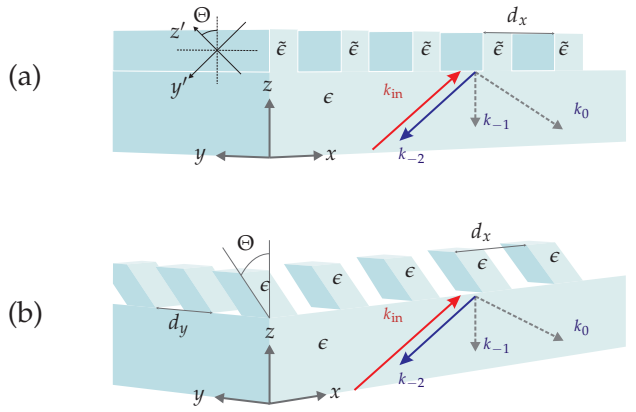

Figure 5.3: (a) The Littrow-half-wave plate in paper III is basically a linear grating made of anisotropic material with rotated anisotropy $\tilde{\epsilon}$. (b) Same physical behaviour is obtained with a crossed slanted structure made in (isotropic) high-refractive index dielectric, such as TiO_2. Wave vectors of the incident and diffracted light lie in the x, z-plane.

diately behind the substrate-grating interface, the 0th component propagating upwards (away from the interface) is in the same polarization $\boldsymbol{P}_1$ as the incident light. Also it is found that the -2nd component propagating downwards (towards the interface) has a new polarization state $\boldsymbol{P}_2$. The relation between $\boldsymbol{P}_1$ and $\boldsymbol{P}_2$ is a half-wave retardation with $\psi = \pm 45^\circ$ as the wave-plate axes.

In other words, the field inside the grating layer consists of two dominating plane-wave components with polarization states $\boldsymbol{P}_1$ and $\boldsymbol{P}_2$, propagating in opposite directions. During propagation back and forth inside the grating layer the energy is coupled between the components. At the substrate-grating interface, the downwards-propagating -2nd component is significantly stronger than the 0th, and is coupled out into the substrate. Hence, we get output light with polarization state $\boldsymbol{P}_2$ propagating oppositely to the incident light.

The behavior is similar to the classical case of two-wave coupling inside volume gratings [102]. Here, the coupling between the differently polarized plane wave components is only possible with the rotated anisotropy, i.e. the slanted grating profile in the y-direction. In paper **III** we present numerical analysis of this effect, and a fabricated prototype element. Figure 5.4 presents a SEM-image of the fabricated element, and a summary of measurement results.

5.4 ACHIRAL OPTICAL ACTIVITY

As mentioned in section 3.3.3 some recent studies have reported optical activity occurring with microstructures with neither intrinsic nor structural chirality [41–43]. In [41] polarization rotation is observed when light is obliquely incident on a two-dimensionally periodic metallic split ring array. In this experiment it was required that the incident wave vector and the orientation of the split ring cells form a chiral three-vector system. This effect has been labeled *extrinsic chirality*.

As the last section of this thesis we present a theoretical result

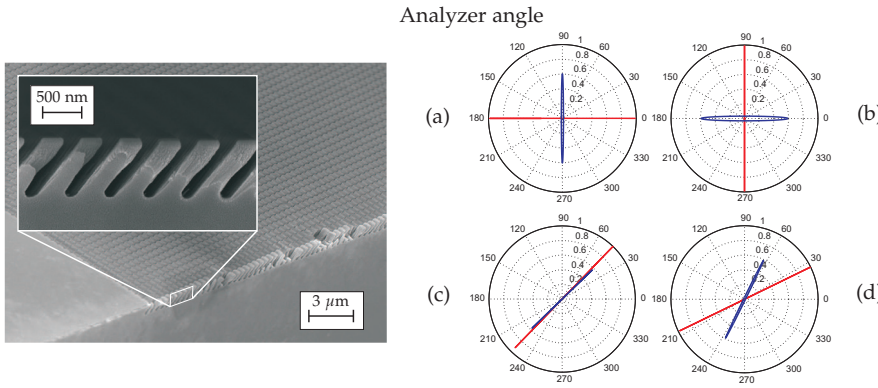

Figure 5.4: On the left, a cross-section SEM-image of the fabricated Littrow-half-wave plate. On the right, measured polarization ellipses of the input (red) and output (blue) beams. Measured with four different input polarizations (a) TM, (b) TE, (c) 45°-linear, and (d) 25°-linear.

about a very strong polarization rotation occurring in a specific diffractive setup. The result has not been achieved experimentally, but numerical analysis has been verified with two different versions of FMM. Furthermore, fabricated gratings with similar shapes were optically measured, SEM-photographed, and re-analyzed numerically. They showed congruence between the numerical method and actual measured data.

The structure (illustrated in Fig. 5.5) is similar to the one in previous section. A slanted pillar grating is made of high refractive index dielectric, such as atomic layer deposited (ALD) titanium dioxide ($n = 2.37$ in our in-house ellipsometric measurements). The grating lies in (x, y)-plane, with grating vectors $d_x = 640$ nm, and $d_y = 410$ nm. The pillar dimensions are $c_x = 220$ nm, $c_y = 275$ nm, and $h = 395$ nm, and the slant angle is $\Theta = 44.2°$. The angle of incidence is $\theta_{\text{in}} = 21.3°$. The used wavelength is again $\lambda = 633$ nm.

The -1st transmitted diffraction order is observed. Both the incident and diffracted wave vectors lie in the (x, z)-plane, since there is no conical rotation in this mounting. Therefore, it is straigthforward to define the coordinate shifts between the local coordinate systems of the incident and diffracted waves. The eigenpolarization method reveals that the Jones matrix for the -1st order with these

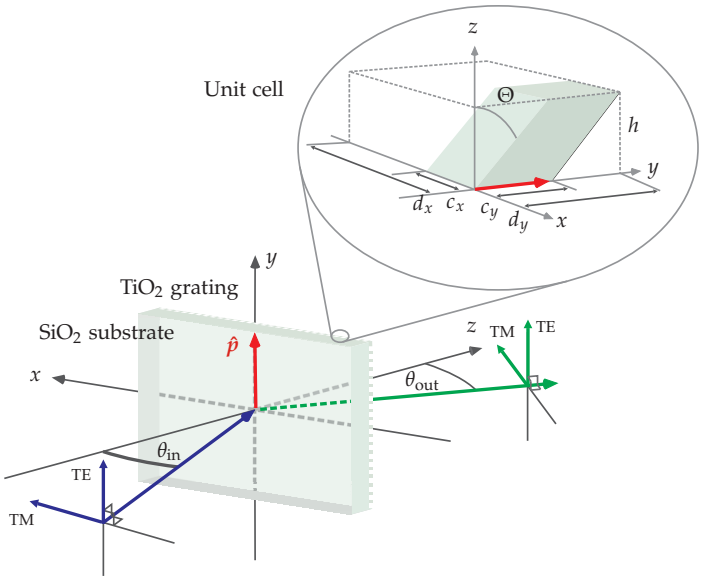

Figure 5.5: Grating geometry of the polarization rotator. Slanted pillar structure made of TiO_2 is on top of a SiO_2 substrate. Polarization states are compared between the incident wave (blue) and the -1st transmitted order (green). Vector $\hat{\mathbf{p}}$ represents the polar direction of the strucure.

exact grating parameters is

$$\mathbf{M}_{-1} = \begin{bmatrix} -0.044 - 0.038\mathrm{i} & -0.919 - 0.500\mathrm{i} \\ 0.880 + 0.470\mathrm{i} & -0.0490 - 0.0270\mathrm{i} \end{bmatrix}, \tag{5.2}$$

which is quite close to the form of a perfect polarization rotator

$$\mathbf{M}_{\mathrm{rot}} = \begin{bmatrix} a + b\mathrm{i} & c + d\mathrm{i} \\ -c - d\mathrm{i} & a + b\mathrm{i} \end{bmatrix}. \tag{5.3}$$

The eigenvectors of M_{-1} are

$$\boldsymbol{V}_1 = \begin{bmatrix} 1 \\ 0.003 + 0.971\mathrm{i} \end{bmatrix}, \text{ and } \boldsymbol{V}_2 = \begin{bmatrix} 1 \\ -0.003 - 0.983\mathrm{i} \end{bmatrix}, \tag{5.4}$$

which are close to right and left handed circular polarizations. The phase difference for $\boldsymbol{V}_1$ and $\boldsymbol{V}_2$ is $\Delta\alpha = -186.3°$.

The fact that the eigenpolarizations are RCP and LCP is extraordinary for a clearly non-chiral structure as this. Further analysis shows that this extrinsic chirality arises from the slanted profile shape. Figure 5.6 illustrates how the eigenpolarizations gradually change from linear to circular as the slant angle is increased. The slanted profile gives the structure a certain polar direction (vector $\boldsymbol{p}$ in Fig. 5.5). The polarity breaks the two-fold rotation symmetry of a non-slanted counterpart. For the extrinsic chirality to appear, (1) the polar direction must be orthogonal to the plane of propagation, (2) oblique incidence must be used, and (3) the observed output must be a non-zeroth diffraction order. This can be seen analogous to the case of metallic split ring structures in [41]. However, the same physical explanation does not apply to any dielectric element.

Figure 5.7 shows the actual polarization rotation and ellipticity as functions of the grating depth for four different linear input

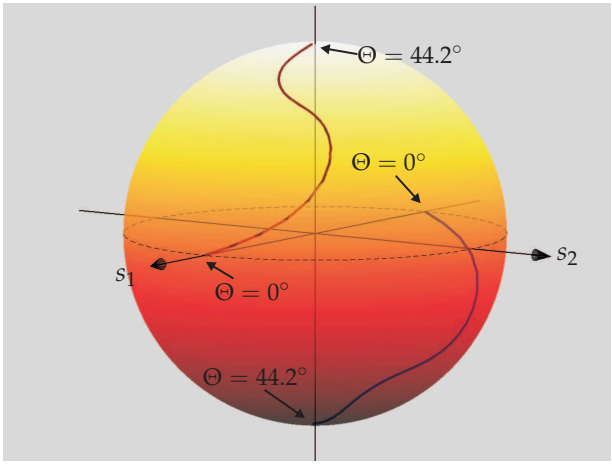

Figure 5.6: Poincare's sphere. Eigenpolarizations (red and blue) of the −1st transmitted order are plotted as the slant angle Θ is varied from 0° to 44.2°. Figure shows how the eigenstates travel, on the surface of the sphere, from TE and TM polarizations to right- and left-handed circular polarizations. Other grating parameters are as listed above.

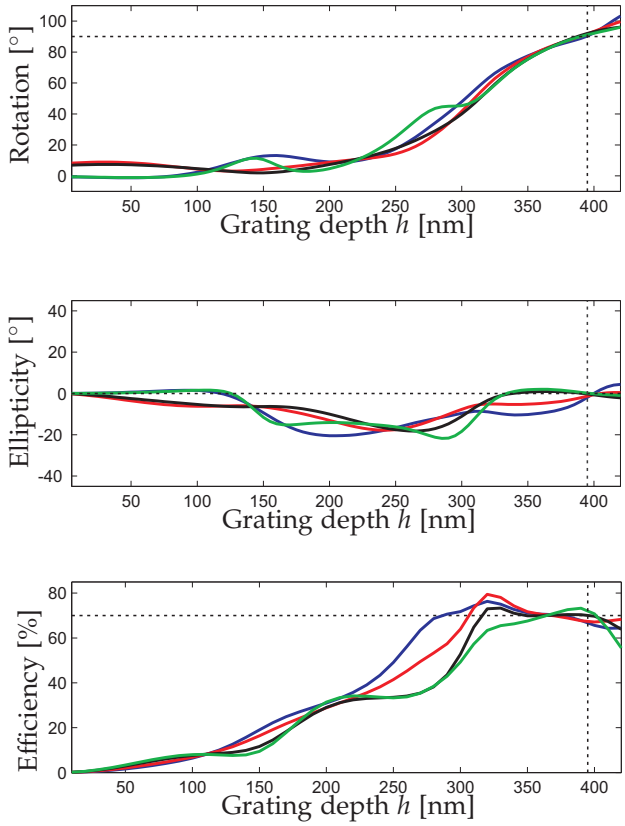

Figure 5.7: Polarization rotation, ellipticity, and efficiency as a function of the grating depth. Plotted for four different incident polarizations: $\psi = 0°$ (blue), $\psi = 30°$ (red), $\psi = 60°$ (black), and $\psi = 90°$ (green).

polarizations. The optimal depth $h = 395$ nm is marked with a dashed line. We see how the grating indeed works like a true optically active media, since the rotation increases steadily and is approximately equal for all input polarizations. The rotation strength is giant, approximately $(140°/\lambda)$.

6 Conclusions

Microstructured elements that provide polarization state manipulation for monochromatic illumination have been the topic of discussion in this thesis. The intention of this work was to find new type of elements to accompany the traditional form-birefringent subwavelength grating.

The subject was approached with the aid of the traditional Jones algebra, rigorous numerical calculations using Fourier modal method, and electron beam lithography. The theory and background of these methods were briefly introduced. The first actual original work came across in section 4.1. Several recent studies around the world have discussed optical activity in obliquely illuminated and/or diffractive setups. Therefore there is a need for ways to determine the eigenpolarizations in such configurations, since the classical method, based solely on structure symmetries, is inadequate. The method presented in this thesis and in paper **IV** combines rigorous grating analysis with FMM and traditional Jones algebra.

A numerical investigation was conducted concerning half-wave retardation for light propagating inside a slab waveguide [**I**]. It was shown that using numerically optimized conical incidence geometry, the required aspect ratios needed for such effect can be reasonable for fabrication.

Then, two grating designs that surpass the possibilities of traditional form-birefringence were presented. Both results are based on using a slanted grating profile, which gives rise to unexpected physical mechanisms. Half-wave retardation in direct transmission was demonstrated experimentally with a significantly shallow grating structure [**II**]. A crossed slanted grating producing half-wave retardation in back-reflected -2nd diffraction order was also experimentally tested [**III**]. For both of these experimental studies, SEM images and optical measurement results were presented.

The eigenpolarization analysis [**IV**] was used for optimizing diffractive configurations for optical activity-like effects in non-chiral structures. It was found that giant polarization rotation strength occurs in the -1st transmitted diffraction order in a certain slanted grating geometry. The result has been verified with different numerical methods, which have been cross-checked with optical measurements from similar structures. The main task in the future is to produce an experimental example of this effect, which is feasible yet challenging. If achieved experimentally, this result would have a huge impact on the popular field of artificial optical activity.

Bibliography

[1] N. Passilly, K. Ventola, P. Karvinen, J. Turunen, and J. Tervo, "Achromatic phase retardation by subwavelength gratings in total internal reflection," *J. Opt. A: Pure Appl. Opt.* **10,** 015001 (2008).

[2] N. Passilly, P. Karvinen, K. Ventola, P. Laakkonen, J. Turunen, and J. Tervo, "Polarization conversion by dielectric subwavelength gratings in conical mounting," *J. Eur. Opt. Soc. Rapid. Publ.* **3** (2008).

[3] I. Newton, *Opticks: or a Treatise of the Reflection, Refractions, Inflexions and Colours* (Royal Society., London, 1704).

[4] T. Young, "The Bakerian lecture: experiments and calculations relative to physical optics," *Philosophical Transactions of the Royal Society of London* **94,** pp. 1–16 (1804).

[5] J. Maxwell, *Treatise on Electricity and Magnetism*, Vol. 2, 3 ed. (Dover Publications., New York, 1954).

[6] E. Wolf, "Einstein's researches on the nature of light," *Optics News* **5,** 24–39 (1979).

[7] A. L. Schawlow and C. H. Townes, "Infrared and optical masers," *Phys. Rev.* **112,** 1940–1949 (1958).

[8] A. Javan, "Theory of a three-level maser," *Phys. Rev.* **107,** 1579–1589 (1957).

[9] T. Maiman, "Stimulated optical radiation in ruby," *Nat.* **187,** 493–494 (1960).

[10] K. Able, "Skylight polarization patterns at dusk influence migratory orientation in birds," *Nat.* **299,** 550–551 (1982).

[11] H. Autrum, *Handbook of Sensory Physiology* (springer -Verlag, Berlin, 1980).

[12] D. S. Kliger, *Polarized Light in Optics and Spectroscopy* (Academic Press Inc., San Diego, 1990).

[13] N. Roberts, T.-H. Chiou, N. J. Marshall, and T. W. Cronin, "A biological quarter-wave retarder with excellent achromaticity in the visible wavelength region," *Nat. Photonics* **3,** 641–644 (2009).

[14] D. C. Flanders, "Submicrometer periodicity gratings as artificial anisotropic dielectrics," *Appl. Phys. Lett.* **42,** 492 –494 (1983).

[15] L. H. Cescato, E. Gluch, and N. Streibl, "Holographic quarterwave plates," *Appl. Opt.* **29,** 3286–3290 (1990).

[16] G. Bryan-Brown, J. Sambles, and M. Hutley, "Polarisation conversion through the excitation of surface plasmons on a metallic grating," *J. Mod. Optic.* **37,** 1227–1232(6) (July 1990).

[17] F. Xu, R.-C. Tyan, P.-C. Sun, Y. Fainman, C.-C. Cheng, and A. Scherer, "Fabrication, modeling, and characterization of form-birefringent nanostructures," *Opt. Lett.* **20,** 2457–2459 (1995).

[18] D. L. Brundrett, E. N. Glytsis, and T. K. Gaylord, "Subwavelength transmission grating retarders for use at 10.6 μm," *Appl. Opt.* **35,** 6195–6202 (1996).

[19] W. Yu, K. Satoh, H. Kikuta, T. Konishi, and T. Yotsuya, "Synthesis of wave plates using multilayered subwavelength structure," *Jpn. J. Appl. Phys.* **43,** L439–L441 (2004).

[20] T. Isano, Y. Kaneda, N. Iwakami, K. Ishizuka, and N. Suzuki, "Fabrication of half-wave plates with subwavelength structures," *Jpn. J. Appl. Phys.* **43,** 5294–5296 (2004).

[21] R. Magnusson, M. Shokooh-Saremi, and E. G. Johnson, "Guided-mode resonant wave plates," *Opt. Lett.* **35,** 2472–2474 (2010).

[22] V. Kettunen and F. Wyrowski, "Reflection-mode phase retardation by dielectric gratings," *Opt. Commun.* **158,** 41 – 44 (1998).

[23] R. A. Watts and J. R. Sambles, "Reflection gratings as polarization converters," *Opt. Commun.* **140,** 179 – 183 (1997).

[24] H. Kikuta, Y. Ohira, and K. Iwata, "Achromatic quarter-wave plates using the dispersion of form birefringence," *Appl. Opt.* **36,** 1566–1572 (1997).

[25] N. Bokor, R. Shechter, N. Davidson, A. A. Friesem, and E. Hasman, "Achromatic phase retarder by slanted illumination of a dielectric grating with period comparable with the wavelength," *Appl. Opt.* **40,** 2076–2080 (2001).

[26] D.-E. Yi, Y.-B. Yan, H.-T. Liu, Si-Lu, and G.-F. Jin, "Broadband achromatic phase retarder by subwavelength grating," *Opt. Commun.* **227,** 49 – 55 (2003).

[27] T. Kämpfe and O. Parriaux, "Depth-minimized, large period half-wave corrugation for linear to radial and azimuthal polarization transformation by grating-mode phase management," *J. Opt. Soc. Am. A* **28,** 2235–2242 (2011).

[28] A. Pors, M. G. Nielsen, G. D. Valle, M. Willatzen, O. Albrektsen, and S. I. Bozhevolnyi, "Plasmonic metamaterial wave retarders in reflection by orthogonally oriented detuned electrical dipoles," *Opt. Lett.* **36,** 1626–1628 (2011).

[29] B. Päivänranta, N. Passilly, J. Pietarinen, P. Laakkonen, M. Kuittinen, and J. Tervo, "Low-cost fabrication of form-birefringent quarter-wave plates," *Opt. Express* **16,** 16334–16342 (2008).

[30] T. Yoshikawa, T. Konishi, M. Nakajima, H. Kikuta, H. Kawata, and Y. Hirai, "Fabrication of 1/4 wave plate by nanocasting lithography," *J. Vac. Sci. Technol. B* **23,** 2939–2943 (2005).

[31] J. J. Wang, X. Deng, X. Liu, A. Nikolov, P. Sciortino, F. Liu, and L. Chen, "Ultraviolet wave plates based on monolithic integration of two fully filled and planarized nanograting layers," *Opt. Lett.* **31,** 1893–1895 (2006).

[32] E. Hendry, T. Carpy, J. Johnston, M. Popland, R. V. Mikhaylovskiy, A. J. Lapthorn, S. M. Kelly, L. D. Barron, N. Gadegaard, and M. Kadodwala, "Ultrasensitive detection and characterization of biomolecules using superchiral fields," *Nat. Nanotechnol.* **5,** 783–787 (2010).

[33] L. D. Barron, *Molecular Light Scattering and Optical Activity* (Cambridge University Press, Cambridge, UK, 2004).

[34] J. B. Pendry, "A chiral route to negative refraction," *Science* **306,** 1353–1355 (2004).

[35] R. Williams, "Optical rotatory effect in the nematic liquid phase of *p*-azoxyanisole," *Phys. Rev. Lett.* **21,** 342–344 (1968).

[36] C. M. Soukoulis, S. Linden, and M. Wegener, "Negative refractive index at optical wavelengths," *Science* **315,** 47–49 (2007).

[37] M. Thiel, G. von Freymann, and M. Wegener, "Layer-by-layer three-dimensional chiral photonic crystals," *Opt. Lett.* **32,** 2547–2549 (2007).

[38] J. Lee and C. Chan, "Polarization gaps in spiral photonic crystals," *Opt. Express* **13,** 8083–8088 (2005).

[39] M. Liu, Y. Zhang, X. Wang, and C. Jin, "Incident-angle-insensitive and polarization independent polarization rotator," *Opt. Express* **18,** 11990–12001 (2010).

[40] X. Meng, B. Bai, P. Karvinen, K. Konishi, J. Turunen, Y. Svirko, and M. Kuwata-Gonokami, "Experimental realization of all-dielectric planar chiral metamaterials with large optical activity in direct transmission," *Thin Solid Films* **516,** 8745 – 8748 (2008).

[41] E. Plum, X.-X. Liu, V. A. Fedotov, Y. Chen, D. P. Tsai, and N. I. Zheludev, "Metamaterials: optical activity without chirality," *Phys. Rev. Lett.* **102,** 113902 (2009).

[42] E. Plum, V. A. Fedotov, and N. I. Zheludev, "Extrinsic electromagnetic chirality in metamaterials," *J. Opt. A: Pure Appl. Opt.* **11,** 074009 (2009).

[43] E. Plum, V. A. Fedotov, and N. I. Zheludev, "Optical activity in extrinsically chiral metamaterial," *Appl. Phys. Lett.* **93,** 191911 –191911–3 (2008).

[44] L. Mandel and E. Wolf, *Optical Coherence and Quantum Optics* (Cambridge University Press, Cambridge, 1995).

[45] K. Knop, "Rigorous diffraction theory for transmission phase gratings with deep rectangular grooves," *J. Opt. Soc. Am.* **68,** 1206–1210 (1978).

[46] L. Li, "Formulation and comparison of two recursive matrix algorithms for modeling layered diffraction gratings," *J. Opt. Soc. Am. A* **13,** 1024–1035 (1996).

[47] R. Petit, *Electromagnetic Theory of Gratings* (springer -Verlag, Berlin, 1980).

[48] J. Turunen, "Diffraction theory of dielectric surface relief gratings," Chap 2 in *Micro-optics: Elements, Systems and Applications*, H. P. Herzig, ed. (Taylor & Francis Inc, Cornwall, 1997).

[49] L. Li, J. Chandezon, G. Granet, and J.-P. Plumey, "Rigorous and efficient grating-analysis method made easy for optical engineers," *Appl. Opt.* **38,** 304–313 (1999).

[50] L. Li, "Note on the S-matrix propagation algorithm," *J. Opt. Soc. Am. A* **20,** 655–660 (2003).

[51] L. Li, "Fourier modal method for crossed anisotropic gratings with arbitrary permittivity and permeability tensors," *J. Opt. A: Pure Appl. Opt.* **5,** 345 (2003).

[52] M. Born and E. Wolf, *Principles of Optics* (Cambridge University Press, Cambridge, UK, 1999).

[53] V. Kettunen, M. Kuittinen, J. Turunen, and P. Vahimaa, "Spectral filtering with finitely conducting inductive grids," *J. Opt. Soc. Am. A* **15,** 2783–2785 (1998).

[54] K. Jefimovs, T. Vallius, V. Kettunen, M. Kuittinen, J. Turunen, P. Vahimaa, M. Kaipiainen, and S. Nenonen, "Inductive grid filters for rejection of infrared radiation," *J. Mod. Opt.* **51,** 1651–1661 (2004).

[55] H. Hertz, *Electric Waves* (Macmillan and Company, London, UK, 1893).

[56] G. R. Bird and J. Maxfield Parrish, "The wire grid as a near-infrared polarizer," *J. Opt. Soc. Am.* **50,** 886 (1960).

[57] B. Schnabel, E.-B. Kley, and F. Wyrowski, "Study on polarizing visible light by subwavelength-period metal-stripe gratings," *Opt. Eng.* **38,** 220–226 (1999).

[58] L. Chen, J. J. Wang, F. Walters, X. Deng, M. Buonanno, S. Tai, and X. Liu, "Large flexible nanowire grid visible polarizer made by nanoimprint lithography," *Appl. Phys. Lett.* **90,** 063111 –063111–3 (2007).

[59] Z. Y. Yang and Y. F. Lu, "Broadband nanowire-grid polarizers in ultraviolet-visible-near-infrared regions," *Opt. Express* **15,** 9510–9519 (2007).

[60] Y. Ekinci, H. H. Solak, C. David, and H. Sigg, "Bilayer Al wire-grids as broadband and high-performance polarizers," *Opt. Express* **14,** 2323–2334 (2006).

[61] J. J. Wang, L. Chen, X. Liu, P. Sciortino, F. Liu, F. Walters, and X. Deng, "30-nm-wide aluminum nanowire grid for ultrahigh contrast and transmittance polarizers made by UV-nanoimprint lithography," *Appl. Phys. Lett.* **89,** 141105 (2006).

[62] "Fabrication of subwavelength aluminum wire grating using nanoimprint lithography and reactive ion etching," *Microelectron. Eng.* **78-79,** 314 – 318 (2005).

[63] J. J. Wang, W. Zhang, X. Deng, J. Deng, F. Liu, P. Sciortino, and L. Chen, "High-performance nanowire-grid polarizers," *Opt. Lett.* **30,** 195–197 (2005).

[64] A. Lehmuskero, I. Vartiainen, T. Saastamoinen, T. Alasaarela, and M. Kuittinen, "Absorbing polarization selective resonant gratings," *Opt. Express* **18,** 27270–27279 (2010).

[65] G. G. Kang, I. Vartiainen, B. F. Bai, H. Tuovinen, and J. Turunen, "Inverse polarizing effect of subwavelength metallic gratings in deep ultraviolet band," *Appl. Phys. Lett.* **99,** 071103 (2011).

[66] C. Menzel, C. Rockstuhl, and F. Lederer, "Advanced Jones calculus for the classification of periodic metamaterials," *Phys. Rev. A* **82,** 053811 (2010).

[67] C. Haggans, L. Li, T. Fujita, and R. Kostuk, "Lamellar gratings as polarization components for specularly reflected beams," *J. Mod. Optic.* **40,** 675–686 (1993).

[68] A. Drezet, C. Genet, and T. W. Ebbesen, "Miniature plasmonic wave plates," *Phys. Rev. Lett.* **101,** 043902 (2008).

[69] J. Yang and J. Zhang, "Subwavelength quarter-waveplate composed of L-shaped metal nanoparticles," *Plasmonics* **6,** 251–254 (2011).

[70] R. L. Dubs, S. N. Dixit, and V. McKoy, "Circular dichroism in photoelectron angular distributions from oriented linear molecules," *Phys. Rev. Lett.* **54,** 1249–1251 (1985).

[71] C. Westphal, J. Bansmann, M. Getzlaff, and G. Schönhense, "Circular dichroism in the angular distribution of photoelectrons from oriented CO molecules," *Phys. Rev. Lett.* **63,** 151–154 (1989).

[72] N. Chandra, "Circular dichroism in photoionization of oriented nonlinear molecules," *Phys. Rev. A* **39,** 2256–2259 (1989).

[73] M. Wegener and S. Linden, "Giving light yet another new twist," *Physics* **2,** 3 (2009).

[74] S. Tretyakov, I. Nefedov, A. Sihvola, S. Maslovski, and C. Simovski, "Waves and energy in chiral nihility," *J. Electromagnet. Wave.* **17,** 695–706 (2003).

[75] J. Dong, J. Zhou, T. Koschny, and C. Soukoulis, "Bi-layer cross chiral structure with strong optical activity and negative refractive index," *Opt. Express* **17,** 14172–14179 (2009).

[76] M. Decker, M. Ruther, C. E. Kriegler, J. Zhou, C. M. Soukoulis, S. Linden, and M. Wegener, "Strong optical activity from twisted-cross photonic metamaterials," *Opt. Lett.* **34,** 2501–2503 (2009).

[77] S. Engelbrecht, M. Wunderlich, A. M. Shuvaev, and A. Pimenov, "Colossal optical activity of split-ring resonator arrays for millimeter waves," *Appl. Phys. Lett.* **97,** 081116 (2010).

[78] M. Decker, R. Zhao, C. M. Soukoulis, S. Linden, and M. Wegener, "Twisted split-ring-resonator photonic metamaterial with huge optical activity," *Opt. Lett.* **35,** 1593–1595 (2010).

[79] A. Papakostas, A. Potts, D. M. Bagnall, S. L. Prosvirnin, H. J. Coles, and N. I. Zheludev, "Optical manifestations of planar chirality," *Phys. Rev. Lett.* **90,** 107404 (2003).

[80] T. Vallius, K. Jefimovs, J. Turunen, P. Vahimaa, and Y. Svirko, "Optical activity in subwavelength-period arrays of chiral metallic particles," *Appl. Phys. Lett.* **83,** 234–236 (2003).

[81] M. Kuwata-Gonokami, N. Saito, Y. Ino, M. Kauranen, K. Jefimovs, T. Vallius, J. Turunen, and Y. Svirko, "Giant optical activity in quasi-two-dimensional planar nanostructures," *Phys. Rev. Lett.* **95,** 227401 (2005).

[82] V. K. Valev, N. Smisdom, A. V. Silhanek, B. De Clercq, W. Gillijns, M. Ameloot, V. V. Moshchalkov, and T. Verbiest, "Plasmonic ratchet wheels: switching circular dichroism by arranging chiral nanostructures," *Nano Lett.* **9,** 3945–3948 (2009).

[83] W. Zhang, A. Potts, A. Papakostas, and D. M. Bagnall, "Intensity modulation and polarization rotation of visible light by dielectric planar chiral metamaterials," *Appl. Phys. Lett.* **86,** 231905 (2005).

[84] W. Zhang, A. Potts, and D. M. Bagnall, "Giant optical activity in dielectric planar metamaterials with two-dimensional chirality," *J. Opt. A: Pure Appl. Opt* **8,** 878 (2006).

[85] B. Bai, K. Konishi, X. Meng, P. Karvinen, A. Lehmuskero, M. Kuwata-Gonokami, Y. Svirko, and J. Turunen, "Mechanism of the large polarization rotation effect in the all-dielectric artificially chiral nanogratings," *Opt. Express* **17,** 688–696 (2009).

[86] M. Decker, M. W. Klein, M. Wegener, and S. Linden, "Circular dichroism of planar chiral magnetic metamaterials," *Opt. Lett.* **32,** 856–858 (2007).

[87] J. K. Gansel, M. Thiel, M. S. Rill, M. Decker, K. Bade, V. Saile, G. von Freymann, S. Linden, and M. Wegener, "Gold helix photonic metamaterial as broadband circular polarizer," *Science* **325,** 1513–1515 (2009).

[88] Z. Fan and A. O. Govorov, "Plasmonic circular dichroism of chiral metal nanoparticle assemblies," *Nano Lett.* **10,** 2580–2587 (2010).

[89] S. N. Volkov, K. Dolgaleva, R. W. Boyd, K. Jefimovs, J. Turunen, Y. Svirko, B. K. Canfield, and M. Kauranen, "Optical activity in diffraction from a planar array of achiral nanoparticles," *Phys. Rev. A* **79,** 043819 (2009).

[90] T. Verbiest, M. Kauranen, Y. Van Rompaey, and A. Persoons, "Optical activity of anisotropic achiral surfaces," *Phys. Rev. Lett.* **77,** 1456–1459 (1996).

[91] S. N. Savenkov, O. I. Sydoruk, and R. S. Muttiah, "Conditions for polarization elements to be dichroic and birefringent," *J. Opt. Soc. Am. A* **22,** 1447–1452 (2005).

[92] S. N. Savenkov, O. I. Sydoruk, and R. S. Muttiah, "Eigenanalysis of dichroic, birefringent, and degenerate polarization elements: a Jones-calculus study," *Appl. Opt.* **46,** 6700–6709 (2007).

[93] N. Bonod, E. Popov, L. Li, and B. Chernov, "Unidirectional excitation of surface plasmons by slanted gratings," *Opt. Express* **15,** 11427–11432 (2007).

[94] B. Wang, J. Jiang, and G. Nordin, "Compact slanted grating couplers," *Opt. Express* **12,** 3313–3326 (2004).

[95] B. Bai, J. Laukkanen, M. Kuittinen, and S. Siitonen, "Optimization of nonbinary slanted surface-relief gratings as high-efficiency broadband couplers for light guides," *Appl. Opt.* **49,** 5454–5464 (2010).

[96] T. Levola and P. Laakkonen, "Replicated slanted gratings with a high refractive index material for in and outcoupling of light," *Opt. Express* **15,** 2067–2074 (2007).

[97] W. Moreau, *Semiconductor Lithography: Principles, Practises, and Materials* (Plenum Press, New York, 1988).

[98] M. Madou, *Fundamentals of Microfabrication: The Science of Miniaturization* (CRC Press LLC, Boca Raton, 2002).

[99] M. A. Vyvoda, H. Lee, M. V. Malyshev, F. P. Klemens, M. Cerullo, V. M. Donnelly, D. B. Graves, A. Kornblit, and J. T. C. Lee, "Effects of plasma conditions on the shapes of features etched in Cl_2 and HBr plasmas. I. Bulk crystalline silicon etching," *J. Vac. Sci. Technol., A* **16,** 3247–3258 (1998).

[100] G. S. Oehrlein, "Reactive Ion etching," Chap 8 in *Handbook of Plasma Processing Technology: Fundamentals, Etching, Deposition, and Surface Interactions*, W. D. W. Stephen M. Rossnagel, J. J. Cuomo, ed. (Noyes Publications., New York, 1990).

[101] *CRC Handbook of Chemistry and Physics* (CRC, 1984).

[102] H. Kogelnik, "Coupled wave theory for thick hologram gratings," *Bell Syst. Tech. J.* **48,** 2909–2947 (1969).

Kalle Ventola

Polarization state manipulation with sub-micron structures

This thesis considers polarization state control using optical structures with sub-micron features. A novel numerical method for optimizing grating structures for polarization effects is presented. Optimization of traditional form-birefingent half-wave retardation in reflection mode is presented. Two novel linear birefringence-like effects with slanted profile gratings are explained and demonstrated experimentally. Large optical activity occuring in a specific mounting of a slanted grating is reported with numerical calculations.

UNIVERSITY OF
EASTERN FINLAND

Publications of the University of Eastern Finland
Dissertations in Forestry and Natural Sciences

ISBN 978-952-61-0979-4 (printed)
ISSNL 1798-5668
ISSN 1798-5668
ISBN 978-952-61-0980-0 (pdf)
ISSN 1798-5676